



## OPEN ACCESS

## EDITED BY

Ian Daly,  
University of Essex, United Kingdom

## REVIEWED BY

Omar Mendoza Montoya,  
Monterrey Institute of Technology and Higher  
Education (ITESM), Mexico  
Usman Ghafoor,  
Pusan National University, Republic of Korea  
Hasan Ayaz,  
Drexel University, United States

## \*CORRESPONDENCE

Kamal Sen  
✉ kamalsen@bu.edu  
Sudan Duwadi  
✉ sudan@bu.edu

## †PRESENT ADDRESS

Matthew Ning,  
Berenson-Allen Center for Noninvasive Brain  
Stimulation, Beth Israel Deaconess Medical  
Center, Boston, MA, United States

RECEIVED 27 October 2023

ACCEPTED 06 March 2024

PUBLISHED 21 March 2024

## CITATION

Ning M, Duwadi S, Yücel MA, von Lühmann A,  
Boas DA and Sen K (2024) fNIRS dataset  
during complex scene analysis.  
*Front. Hum. Neurosci.* 18:1329086.  
doi: 10.3389/fnhum.2024.1329086

## COPYRIGHT

© 2024 Ning, Duwadi, Yücel, von Lühmann,  
Boas and Sen. This is an open-access article  
distributed under the terms of the [Creative  
Commons Attribution License \(CC BY\)](#). The  
use, distribution or reproduction in other  
forums is permitted, provided the original  
author(s) and the copyright owner(s) are  
credited and that the original publication in  
this journal is cited, in accordance with  
accepted academic practice. No use,  
distribution or reproduction is permitted  
which does not comply with these terms.

# fNIRS dataset during complex scene analysis

Matthew Ning<sup>1†</sup>, Sudan Duwadi<sup>1\*</sup>, Meryem A. Yücel<sup>1</sup>,  
Alexander von Lühmann<sup>1,2,3</sup>, David A. Boas<sup>1</sup> and Kamal Sen<sup>1\*</sup>

<sup>1</sup>Department of Biomedical Engineering, Neurophotonics Center, Boston University, Boston, MA, United States, <sup>2</sup>BIFOLD – Berlin Institute for the Foundations of Learning and Data, Berlin, Germany,

<sup>3</sup>Intelligent Biomedical Sensing (IBS) Lab, Technical University Berlin, Berlin, Germany

## KEYWORDS

**open access, fNIRS, spatial attention, complex scene analysis, BCI**

## Introduction

The human brain is an astonishingly powerful computational device, capable of feats yet to be matched by machines. One impressive example is the brain's ability to selectively attend to specific objects in a complex scene with multiple objects. For example, at a crowded cocktail party, we can look at a friend and hear what they are saying in the midst of other speakers, music, and background noise. Such multisensory filtering allows us to select and process important objects in a complex scene, a process known as Complex Scene Analysis (CSA) (Cherry, 2005; Haykin and Chen, 2005; McDermott, 2009). In stark contrast, millions of humans worldwide with disorders such as ADHD (Mihali et al., 2018; Fu et al., 2022), autism (Marco et al., 2011; Lolk, 2013), and hearing losses (Marrone et al., 2008) find such complex scenes confusing, overwhelming and debilitating. Thus, brain-computer interfaces (BCIs) and assistive devices for CSA have the potential to improve the quality of life for many humans.

Recently, we proposed a brain-inspired algorithm for auditory scene analysis based on a model of cortical neurons (Maddox et al., 2012; Dong et al., 2016; Chou et al., 2022). This algorithm has the potential to be applied in assistive devices for CSA. However, a critical piece of information required by the algorithm is the spatial location of the target stimulus. Thus, a portable and non-invasive technology that can decode the spatial location of the attended target stimulus during CSA would greatly facilitate the development of BCIs and assistive devices for CSA. In addition, a technology that provides insights into specific brain regions that play a significant role in decoding the attended location has the potential to advance our understanding of fundamental brain mechanisms underlying CSA in both normal and impaired humans.

Functional near-infrared spectroscopy (fNIRS) is a non-invasive neuroimaging technique that measures changes in oxygenated (HbO<sub>2</sub>) and deoxygenated hemoglobin (HbR) in the cerebral cortex (Chance et al., 1993; Girouard and Iadecola, 2006). Due to its portability and low cost, fNIRS has been used in Brain-Computer Interface (BCI) applications (Naseer and Hong, 2015). Previously, fNIRS has been applied to various aspects of auditory science such as classifying different sound categories (Hong and Santosa, 2016), identifying spatial locations of noise stimuli (Tian et al., 2021), characterizing hemodynamic responses to varying auditory stimuli (Pollonini et al., 2014; Steinmetzger et al., 2020; Luke et al., 2021), and investigating informational masking

([Zhang et al., 2018, 2021](#)). However, to date, fNIRS has not been applied to decode auditory and visual-spatial attention during CSA, and thus, no such dataset exists yet.

Here, we collected brain signals with fNIRS during the presentation of audio-visual stimuli in the presence of competing stimuli from multiple locations in order to mimic complex natural scenes. We targeted the dorsal frontoparietal network including frontal eye field (FEF) and intraparietal sulcus (IPS) as well as superior temporal gyrus/planum temporale (STG/PT), which were shown to be activated by auditory, visual, or audio-visual spatial tasks in fMRI ([Shomstein and Yantis, 2006](#); [Deouell et al., 2007](#); [Wu et al., 2007](#); [Smith et al., 2010](#); [Van der Zwaag et al., 2011](#); [Michalka et al., 2015, 2016](#)) and simultaneous magnetoencephalography (MEG)/electroencephalogram (EEG) studies ([Larson and Lee, 2013](#)). We also recorded task performance by asking the subjects to identify the content of audio-visual stimuli that they were asked to attend to.

Both visual and auditory cues play an important role in CSA. One important observation made in the last few decades is that visual and auditory modalities can influence each other as shown in psychophysical, neurophysiological, and neuroimaging studies. These studies suggest the idea that perception combines features from both visual stimuli and auditory stimuli to form a single auditory-visual object ([Bizley et al., 2016](#)). Both auditory and visual features can contribute cross-modally to enhance auditory or visual object formation, which in turn, can enhance attention operating on auditory ([Busse et al., 2005](#); [Serences et al., 2005](#); [Shomstein and Yantis, 2006](#); [Maddox et al., 2015](#)) or visual objects ([Desimone and Duncan, 1995](#); [Knudsen, 2007](#)). Cross-modal influences have been demonstrated via activation or modulation in primary visual cortex by auditory stimuli ([Petro et al., 2017](#)), single-unit and local field potential modulation in primary auditory cortex by visual stimuli ([Bizley et al., 2007](#); [Kayser et al., 2008](#)) and fMRI study on humans ([Calvert et al., 1999, 2001](#); [Laurienti et al., 2002](#); [Martuzzi et al., 2006](#)). Thus, employing auditory-visual objects to investigate CSA has the potential to reveal additional aspects of CSA beyond paradigms that utilize auditory stimuli alone, e.g., EEG-based auditory attention decoding algorithms. Our experimental paradigm uses multiple videos of individual speakers talking to simulate a cocktail party like setting. We also employ fNIRS to decode the attended location. fNIRS has higher spatial resolution and is less prone to movement artifacts compared to EEG. Moreover, fNIRS enables the measurement of brain activity under less restricted conditions compared to fMRI where subjects are required to be in a supine position. Thus, fNIRS has the potential to complement these other modalities to provide insight into CSA in more naturalistic settings.

This report provides an open-access fNIRS dataset that can be used to develop, test, and compare machine learning algorithms for classifying attended locations based on the fNIRS signals on a single trial basis. In total, we have collected ~990 trials in 11 subjects (30 trials in each condition for 3 conditions, 90 trials per subject for 11 subjects). Our sample preliminary analysis using Linear Discriminant Analysis (LDA) shows robust decoding of attended spatial location for more than half of our subjects for two class classification (individual subject accuracy provided in [Table 1](#)), demonstrating its potential for BCI systems in noisy

environments. This dataset will be available for scientists and students for further analysis and exploration and enable posing and testing new hypotheses regarding spatial information processing. Analysis code for two-class and three-class classification performed in this paper is publicly available on GitHub at [https://github.com/NSNC-Lab/fNIRS\\_DecodingSpatialAttention](https://github.com/NSNC-Lab/fNIRS_DecodingSpatialAttention).

## Methods

### Participants and demographics

Sixteen adults with normal hearing (age 19–48, 8 males and 8 females) were recruited for this study in accordance with the Institutional Review Board of Boston University, out of which only 11 (five males and six females) were included in analysis after exclusion criteria (exclusion criteria details are provided on [Table 1](#) caption). A COVID-19 protocol was developed and strictly adhered to. Participants were screened to exclude those with history of major head trauma or neurological or psychiatric disorder, those who are taking psychoactive medication, those with facial or scalp eczema, those with abnormal or non-contact-corrected vision, and those with abnormal hearing or hearing impairment. Participants were briefed and consented before partaking in this study and were compensated for their time.

### Experimental paradigm

Participants were seated in front of 3 monitors, located at locations equidistant from the subject: center or 0°, 45° to the left, and 45° to the right. The subjects were instructed to rest their chin on a chin rest throughout the experiment to discourage head movements. The subjects were asked to refrain from movements during the tasks except for answering the questions at the end of each trial. The auditory stimuli were delivered via an earphone (ER-1 Etymotic Research Inc.) with ear tips (E-A-RLink 3A Insert Eartips), and corresponding videos were displayed on the monitors. The videos used in the experiment are from AVSpeech, a publicly available dataset ([Ephrat et al., 2018](#), <https://looking-to-listen.github.io/avspeech/index.html>). Videos were screened to include only those with English language and only those where speakers are alone in the videos. In the case there were two people in the video, strictly, only one person was talking. For each trial, a 2-s long audio-visual cue was delivered randomly at one of the 3 locations in the form of a white cross against a black background and a 2 kHz pure tone linearly ramped in the first 0.5 s. The subjects were instructed to listen to the cue and pay attention to the speaker at the cued location. The cue was followed by three videos, one for each location, one of which was the target speaker, and the remaining two were the maskers. The stimuli were followed by two multiple-choice questions on the center monitor, each question containing five possible choices. The first question was related to face identification, and the second was related to transcript identification. In the face identification task, the subjects were presented with five different faces and were tasked with correctly identifying the face of the target speaker shown

TABLE 1 Individual subject behavioral performance, classification accuracy, and statistics.

Subjects	Audio and visual correctness (%)	Number of channels pruned (at SNR 1.5)	CV accuracy in percentage (2 class)	CV accuracy in percentage (3 class)	One way ANOVA statistics for three class features			
					ANOVA (F-statistic, p-value)	Between class p-values		
						Left (L) and Right (R)	Left (L) and Center (C)	Right (R) and Center (C)
8	94.44	2	95	67	(35.86, 4.18e-16)	(L,R, 1.03e-4)	(L,C, 4.3e-17)	(R,C, 2.87e-5)
10	48.89	12	55	34	(4.58, 0.103)	(L,R, 0.2026)	(L,C, 0.4145)	(R, C, 0.0073)
12	93.33	18	92	84	(21.71, 4.36e-10)	(L,R, 3.26e-10)	(L,C, 6.82e-5)	(R, C, 0.0612)
13	96.67	8	60	33	(1.19, 0.305)	(L,R, 0.6038)	(L,C, 0.2766)	(R, C, 0.8217)
14	77.78	10	66	46	(18.61, 1.02e-8)	(L,R, 0.3267)	(L,C, 9.81e-9)	(R, C, 3.46e-4)
15	74.44	2	55	35	(30.39, 9.41e-14)	(L,R, 3.6e-7)	(L,C, 2.51e-14)	(R, C, 0.0174)
16	94.44	11	92	62	(24.3, 3.38e-11)	(L,R, 1.9e-9)	(L,C, 0.9417)	(R, C, 1.06e-8)
17	80	21	68	33	(3.73, 0.242)	(L,R, 0.0334)	(L,C, 0.9546)	(R, C, 0.0614)
18	96.67	20	65	33	(7.85, 0.004)	(L,R, 2.305e-4)	(L,C, 0.1282)	(R, C, 0.1149)
19	96.67	7	83	42	(6.55, 0.0015)	(L,R, 0.0058)	(L,C, 0.0043)	(R, C, 0.9998)
20	83.33	25	66	49	(0.07, 0.93)	(L,R, 0.9943)	(L,C, 0.9521)	(R, C, 0.9363)
21	81.11	19	86	55	(1.09, 0.336)	(L,R, 0.3164)	(L,C, 0.5264)	(R, C, 0.8999)
22	78.89	5	75	40	(11.98, 6.63e-6)	(L,R, 6.27e-7)	(L,C, 0.0012)	(R, C, 0.3530)
23	78.89	18	65	46	(7.31, 0.0007)	(L,R, 0.0016)	(L,C, 0.9591)	(R, C, 0.0033)
24	95.56	6	92	33	(9.06, 0.0001)	(L,R, 2.51e-4)	(L,C, 0.9344)	(R, C, 0.0018)
25	48.89	12	50	30	(8.31, 0.0003)	(L,R, 0.2033)	(L,C, 0.0299)	(R, C, 2.16e-4)

Subjects highlighted in green are included and the ones highlighted in red are excluded. The criteria for exclusion are the number of channels pruned at SNR 1.5 - if 20 or more channels are pruned, they are excluded from further analysis, and behavioral response correctness - if they scored below 70% in both face and transcript identification tasks. One way ANOVA test was performed to compare features for left, right, and center conditions. F-statistic and p-values are reported for ANOVA, and between class comparisons p-values are reported using Tukey-Kramer method in MATLAB.

in the video (“Who was the target speaker?”). In the transcript identification task, the subjects were presented with five different transcripts and were tasked with correctly identifying the transcript spoken by the target speaker in the video (“What was the target speaker saying?”). A trial was counted as correct if the participant correctly identified both the face and the transcript spoken by the target speaker. Upon the completion of two questions, a blank black screen of jittered duration with uniform distribution between 14 and 16 seconds appeared. Thereafter, an instruction to press the spacebar to begin the next trial was displayed on the center monitor. While the audio-visual cue and the video clip lasted 2 and 3 s respectively, the subjects had 20 s in total to answer both multiple-choice questions, but they could move on to the next trial by pressing the space bar immediately after they finished answering. **Figure 1** shows the schematic of experiment setup and the timeline of trial progression.

## Data acquisition

fNIRS data were collected using continuous wave fNIRS (CW6, Techen System) using 690 nm and 830 nm wavelengths, with a 50 Hz sampling rate. Multiple channels were supported with frequency multiplexing. The fNIRS recording software was synced to the stimulus presentation with the Neurospec MMB70-817 triggerbox (Neurospec AG, Switzerland). Fifty-six cm Landmark Cap (EasyCap, Herrsching, Germany) was used for all the subjects.

## Measurements

### fNIRS probe design

The probe (optode array) was designed in publicly available AtlasViewer software (<https://github.com/BUNPC/AtlasViewer>) (Aasted et al., 2015). The probe contains 12 sources, 17 long-separation detectors, and 6 short-separation detectors (SS), for a total of 30 long-separation channels (with an exception for one subject who had 14 sources, 19 long-separation detectors, and 8 short-separation detectors, for a total of 34 long-separation channels). The long-separation detectors were placed 30 mm from the sources whereas SS detectors were placed 8 mm from the sources. The probe covered the dorsal frontoparietal network including the frontal eye field (FEF) and intra-parietal sulcus (IPS) as well as the superior temporal gyrus/plenum temporal (STG/PT). **Figures 2A, B** shows the sensitivity profile for the fNIRS probe geometry.

## Data structure and format

The fNIRS dataset consists of 90 trials each for 11 subjects. The behavioral dataset consists of recorded responses of the subject during each trial and actual answers to the questions asked to the subjects during each trial. fNIRS dataset is in “.snirf” format, and the behavioral dataset is in “.mat” format. Brain Imaging Data Structure (BIDS) compliant fNIRS dataset can be found on OpenNeuro (doi: [10.18112/openneuro.ds004830.v1.0.0](https://doi.org/10.18112/openneuro.ds004830.v1.0.0)).

The behavioral dataset and the data structure details for both fNIRS and behavioral data can be found in the derivatives folder under “Experimental and Behavioral Dataset description.docx.”

## Preliminary analysis and data quality assessment

Preliminary fNIRS data preprocessing and analysis were done using publicly available Homer3 software (<https://github.com/BUNPC/Homer3>) (Huppert et al., 2009). Version of the Homer software used for preliminary analysis is included in GitHub along with custom scripts. Baseline classification analysis using LDA was done using custom code provided at: [https://github.com/NSNC-Lab/fNIRS\\_DecodingSpatialAttention](https://github.com/NSNC-Lab/fNIRS_DecodingSpatialAttention).

### Signal-to-noise ratio

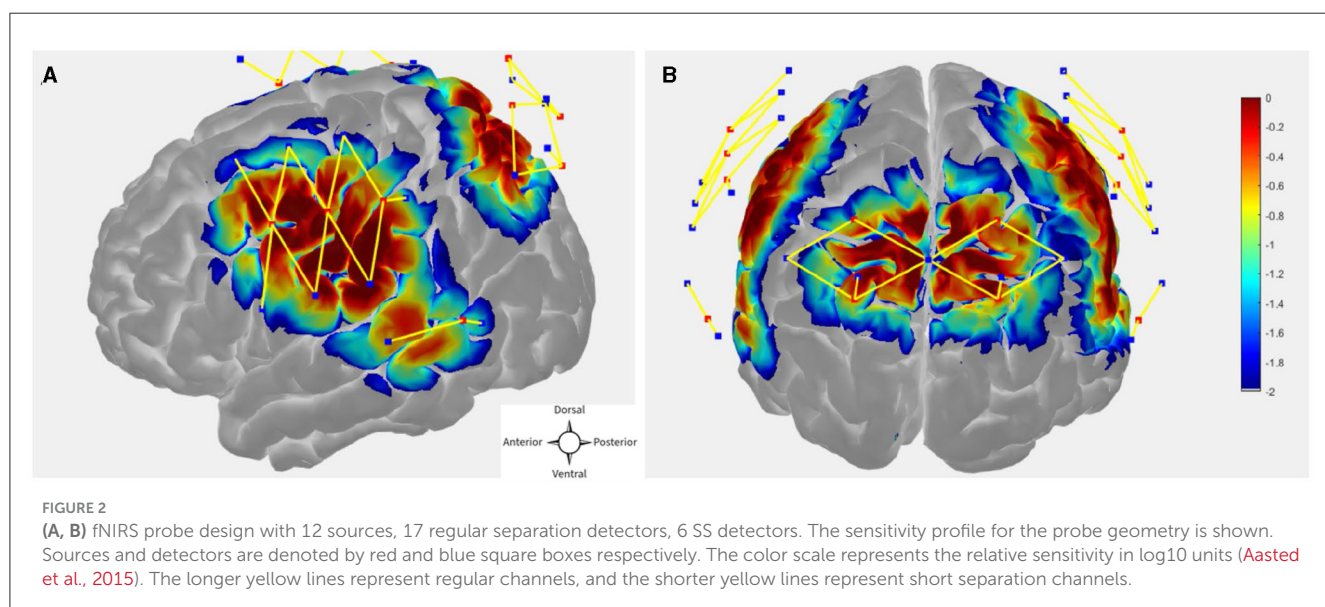
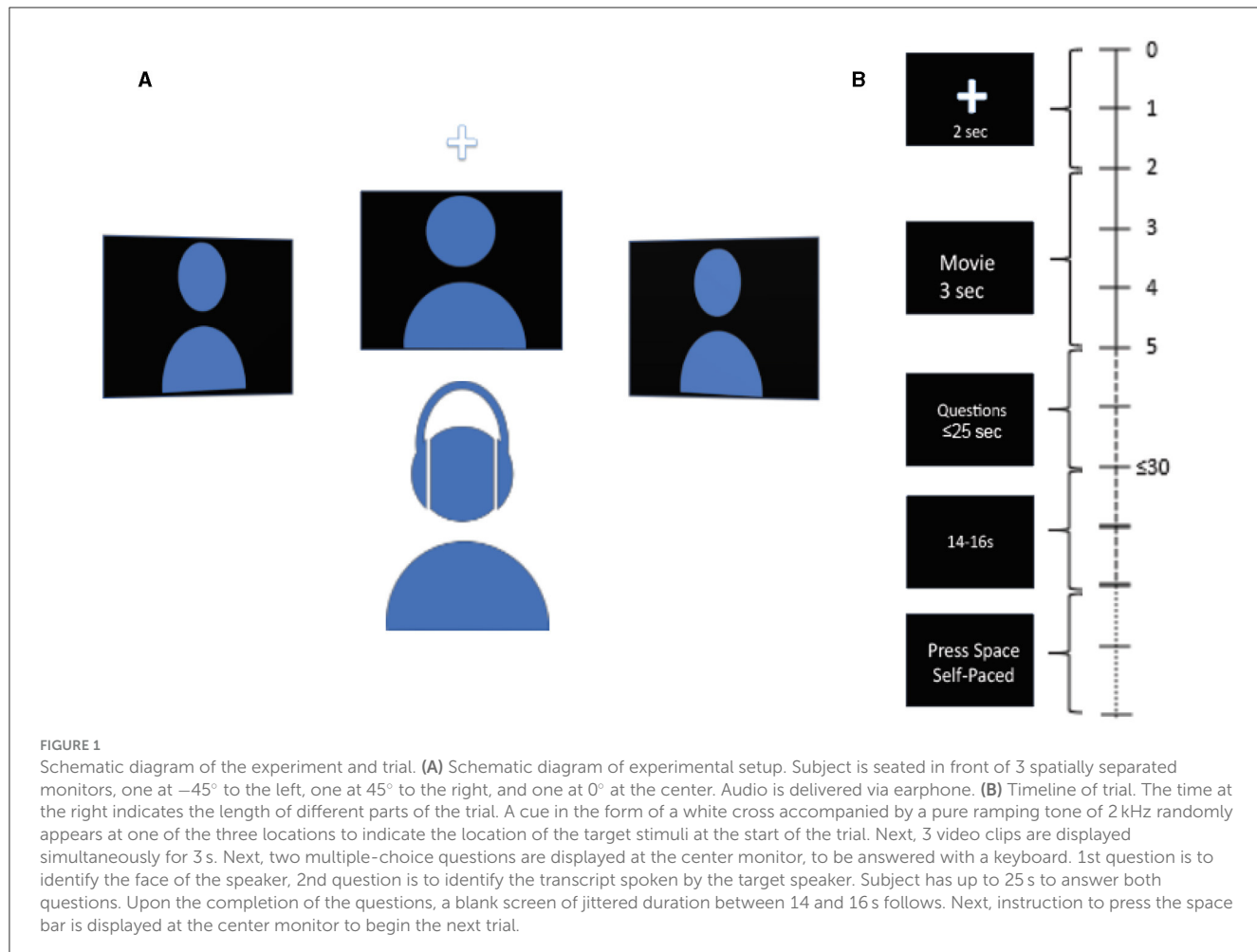
We excluded subjects that had at least 20 channels pruned using a cutoff of  $\text{SNR} = 1.5$ , where SNR was estimated as the mean divided by the standard deviation of raw intensity of the fNIRS signal.

### fNIRS pre-processing

Raw light intensities were converted to optical densities using the mean signal as the arbitrary reference point. Motion artifacts in optical density (OD) were identified and corrected with targeted Principal Component Analysis (PCA) before applying criteria for automatic rejection of stimulus trials (Yücel et al., 2014). OD signals were band-pass filtered between 0.01 Hz and 0.5 Hz with a 3rd order zero-phase Butterworth filter. The filtered OD was converted to chromophore concentration changes. The differential path length factor was held fixed at 1, and the concentration unit is in Molar\*mm (Scholkmann and Wolf, 2013). Finally, systemic physiological signal clutter was regressed out using a GLM with short-separation channels modeling the signal clutter (Gagnon et al., 2014; von Lüthmann et al., 2020). Each regular channel was assigned an SS channel with the highest correlation (Gagnon et al., 2014).

For Hemodynamic response function (HRF) modeling, we fitted the GLM model to each subject. The GLM fitting here used two classes of regressors: HRF for each condition and the systemic signal clutter. The temporal basis functions used to model the HRF consisted of a sequence of 16 Gaussian functions, spaced 1 s apart, with a typical width of 1 s (Gagnon et al., 2011). This flexible model offers better fitting of the HRF shape at the expense of more parameter estimations than the typical canonical hemodynamic response function (Lindquist et al., 2009). Short-separation (SS) fNIRS signals were used as physiological regressors.

Fitting the GLM regression model to the entire data first before cross-validating the trials would result in information leakage (von Lüthmann et al., 2020). In order to avoid leakage, we cross-validated both the GLM regression and classification steps. In each fold of the



cross-validation, we fitted the GLM model to a training dataset and estimated regression coefficients using the Ordinary Least Squares (OLS) method. Then the short separation regression coefficients (SS

coefficients) estimated from the training set are used for the test set where the individual trials are the difference between the measured fNIRS signals and the systemic physiological regressor weighted

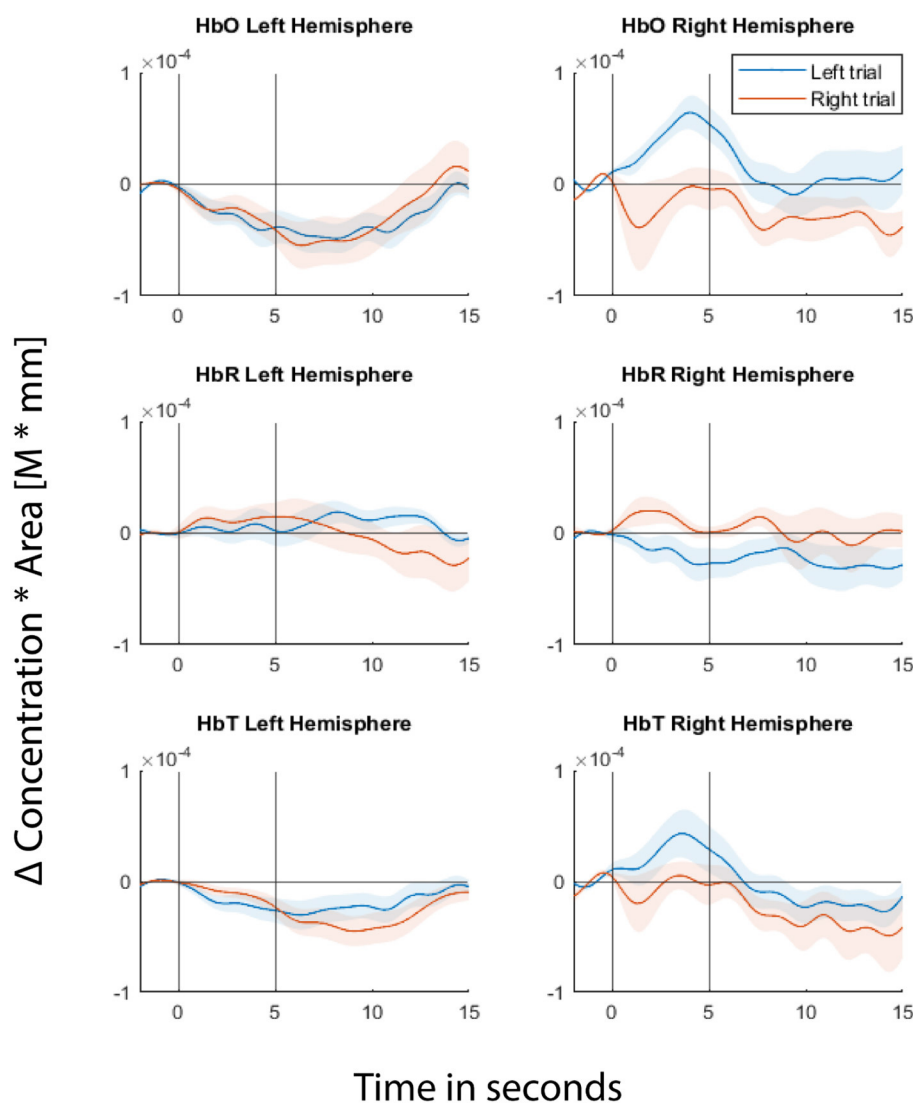


FIGURE 3

Hemodynamic Response Functions (HRFs) of two of the example channels, one from each hemisphere. Top panel represents  $\Delta(\text{HbO})$ , middle panel represents  $\Delta(\text{HbR})$ , and bottom panel represents  $\Delta(\text{HbT})$ . Left column represents the channel from the left hemisphere and the right column represents the channel from the right hemisphere. Blue line represents GLM-fitted HRF responses to left stimuli and red line for right stimuli. Shaded regions represent 95% confidence intervals. The first black vertical line at 0th second represents the cue onset and the second vertical black line represents the movie offset. The movie starts at the 2nd second.

by the SS coefficients. Figure 3 shows the GLM fitted group level HRF for one of the example channels from each hemisphere for the readers to visualize the signals from which the features were extracted during classification.

Table 1 shows individual subject's data. It consists of behavioral data in terms of correctness of responses in both face and transcript identification tasks, number of channels pruned at SNR threshold of 1.5, individual subject's CV accuracy, and one way ANOVA results.

## Classification

As a baseline analysis, we used LDA with linear shrinkage of the covariance matrix (Ledoit and Wolf, 2004). We tested

2-class classification between left ( $-45^\circ$ ) and right ( $45^\circ$ ) spatial locations. The features used were the area under the curve of the Hemodynamic Response Function (HRF) with total hemoglobin (HbT). The features were used from an incremental window where all windows start at 0th second (cue onset). Window lengths tested here are 0 to 0.1, 0.2, 0.5, 1, 1.5, 2, 3, 4, and 5 s. We performed 10 repetitions of 5-fold nested cross-validation (CV). Classifier test performance metric used is Cross Validation accuracy. We achieved a mean CV accuracy of  $\sim 73\%$  for 2 classes and  $\sim 45\%$  for 3 class classification at 5 seconds window. Table 1 shows the individual subject accuracy for both 2 class and 3 class classification. Figure 4 shows the average CV accuracy across the subjects when all of the channels were used (from all targeted regions of interest).

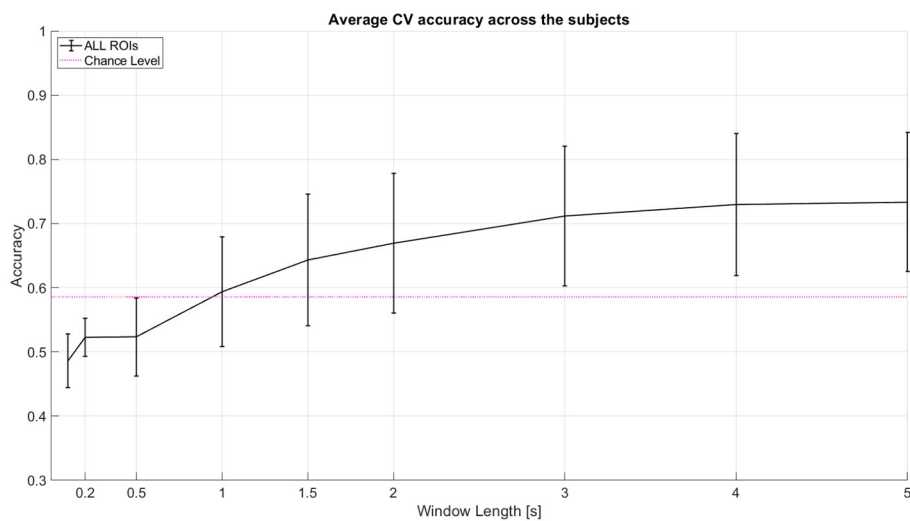


FIGURE 4

Average CV accuracy across 11 subjects when all regions of interest (ROI) are considered. All windows start at 0 s (cue onset). Decision window lengths tested here are 0 to 0.1, 0.2, 0.5, 1, 1.5, 2, 3, 4, and 5 s. The pink line indicates statistical significance for  $p = 0.05$  using a two-tailed  $t$ -test and the given standard deviation from our cross-validation accuracies across subjects at window length 1 s. Error bars represent 95% confidence intervals (counting each subject's model performance accuracy as one sample point).

## Summary

Here, we presented an fNIRS dataset from 11 subjects, along with a behavioral dataset for decoding of attended audio-visual location. We include the custom MATLAB scripts for two-class and three-class classification. We also provide a link to the pre-processing code repository that includes any modification to the Master Homer3 package. This dataset can be used to train, test, and validate machine learning models for attention-based BCIs on a single trial basis.

## Data availability statement

The datasets presented in this study can be found in online repositories. The names of the repository/repositories and accession number(s) can be found in the article/supplementary material.

## Ethics statement

The studies involving humans were approved by the Boston Medical Center and Boston University Medical Campus Institutional Review Board. The studies were conducted in accordance with the local legislation and institutional requirements. The participants provided their written informed consent to participate in this study.

## Author contributions

MN: Data curation, Methodology, Software, Visualization, Writing – original draft, Writing – review & editing. SD: Software,

Visualization, Writing – original draft, Writing – review & editing. MY: Methodology, Supervision, Writing – review & editing. AVL: Methodology, Writing – review & editing. DB: Methodology, Writing – review & editing. KS: Conceptualization, Supervision, Writing – review & editing.

## Funding

The author(s) declare that financial support was received for the research, authorship, and/or publication of this article. T32 grant support for MN from the National Institutes of Health (5T32DC013017-03), Dean's Catalyst Award from the College of Engineering, Boston University, to DB and KS, an award from the American Hearing Research Foundation to DB and KS, and an NSF award #2319321 to KS.

## Conflict of interest

The authors declare that the research was conducted in the absence of any commercial or financial relationships that could be construed as a potential conflict of interest.

The author(s) declared that they were an editorial board member of Frontiers, at the time of submission. This had no impact on the peer review process and the final decision.

## Publisher's note

All claims expressed in this article are solely those of the authors and do not necessarily represent those of their affiliated

organizations, or those of the publisher, the editors and the reviewers. Any product that may be evaluated in this article, or

claim that may be made by its manufacturer, is not guaranteed or endorsed by the publisher.

## References

Aasted, C. M., Yücel, M. A., Cooper, R. J., Dubb, J., Tsuzuki, D., Becerra, L., et al. (2015). Anatomical guidance for functional near-infrared spectroscopy: AtlasViewer tutorial. *Neurophotonics* 2, 020801–020801. doi: 10.1117/1.NPh.2.2.020801

Bizley, J. K., Maddox, R. K., and Lee, A. K. C. (2016). Defining auditory-visual objects: behavioral tests and physiological mechanisms. *Trends Neurosci.* 39, 74–85. doi: 10.1016/j.tins.2015.12.007

Bizley, J. K., Nodal, F. R., Bajo, V. M., Nelken, I., and King, A. J. (2007). Physiological and anatomical evidence for multisensory interactions in auditory cortex. *Cereb. Cortex* 17, 2172–2189. doi: 10.1093/cercor/bhl128

Busse, L., Roberts, K. C., Crist, R. E., Weissman, D. H., and Woldorff, M. G. (2005). The spread of attention across modalities and space in a multisensory object. *Proc. Nat. Acad. Sci.* 102, 18751–18756. doi: 10.1073/pnas.0507704102

Calvert, G. A., Brammer, M. J., Bullmore, E. T., Campbell, R., Iversen, S. D., David, A. S., et al. (1999). Response amplification in sensory-specific cortices during crossmodal binding. *NeuroReport* 10, 2619–2623. doi: 10.1097/00001756-199908200-00033

Calvert, G. A. C., Iversen, S. D., and Brammer, M. J. (2001). Detection of audio-visual integration sites in humans by application of electrophysiological criteria to the BOLD Effect. *NeuroImage* 14, 427–438. doi: 10.1006/nimg.2001.0812

Chance, B., and Zhuang, Z., UnAh, C., Alter, C., and Lipton, L. (1993). Cognition-activated low-frequency modulation of light absorption in human brain. *Proc. Nat. Acad. Sci. U. S. A.* 90, 3770–3774. doi: 10.1073/pnas.90.8.3770

Cherry, E. C. (2005). Some experiments on the recognition of speech, with one and with two ears. *The J. Acous. Soc. Am.* 25, 975–979. doi: 10.1121/1.1907229

Chou, K. F., Boyd, A. D., Best, V., Colburn, H. S., and Sen, K. (2022). A biologically oriented algorithm for spatial sound segregation. *Front. Neurosci.* 16:1004071. doi: 10.3389/fnins.2022.1004071

Deouell, L. Y., Heller, A. S., Malach, R., D'Esposito, M., and Knight, R. T. (2007). Cerebral responses to change in spatial location of unattended sounds. *Neuron* 55, 985–996. doi: 10.1016/j.neuron.2007.08.019

Desimone, R., and Duncan, J. (1995). Neural mechanisms of selective visual attention. *Ann. Rev. Neurosci.* 18, 193–222. doi: 10.1146/annurev.ne.18.030195.001205

Dong, J., Colburn, H. S., and Sen, K. (2016). Cortical transformation of spatial processing for solving the cocktail party problem: a computational model. *eNeuro* 3:ENEURO.0086-15.2015. doi: 10.1523/ENEURO.0086-15.2015

Ephrat, A., Mosseri, I., Lang, O., Dekel, T., Wilson, K., Hassidim, A., et al. (2018). Looking to listen at the cocktail party. *ACM Trans. Graph.* 37, 1–11. doi: 10.1145/3197517.3201357

Fu, T., Li, B., Yin, W., Huang, S., Liu, H., Song, Y., et al. (2022). Sound localization and auditory selective attention in school-aged children with ADHD. *Front. Neurosci.* 16:1051585. doi: 10.3389/fnins.2022.1051585

Gagnon, L., Perdue, K., Greve, D. N., Goldenholz, D., Kaskhedikar, G., Boas, D. A., et al. (2011). Improved recovery of the hemodynamic response in diffuse optical imaging using short optode separations and state-space modeling. *NeuroImage* 56, 1362–1371. doi: 10.1016/j.neuroimage.2011.03.001

Gagnon, L., Yücel, M. A., Boas, D. A., and Cooper, R. J. (2014). Further improvement in reducing superficial contamination in fNIRS using double short separation measurements. *NeuroImage* 85, 127–135. doi: 10.1016/j.neuroimage.2013.01.073

Girouard, H., and Iadecola, C. (2006). Neurovascular coupling in the normal brain and in hypertension, stroke, and Alzheimer disease. *J. Appl. Physiol.* 100, 328–335. doi: 10.1152/japplphysiol.00966.2005

Haykin, S., and Chen, Z. (2005). The cocktail party problem. *Neural Comp.* 17, 1875–1902. doi: 10.1162/0899766054322964

Hong, K. S., and Santosa, H. (2016). Decoding four different sound-categories in the auditory cortex using functional near-infrared spectroscopy. *Hearing Res.* 333, 157–166. doi: 10.1016/j.heares.2016.01.009

Huppert, T. J., Diamond, S. G., Franceschini, M. A., and Boas, D. A. (2009). HomER: a review of time-series analysis methods for near-infrared spectroscopy of the brain. *Applied Optics* 48, D280–D298. doi: 10.1364/AO.48.0D280

Kayser, C., Petkov, C. I., and Logothetis, N. K. (2008). Visual modulation of neurons in auditory cortex. *Cereb Cortex* 18, 1560–1574. doi: 10.1093/cercor/bhm187

Knudsen, E. I. (2007). Fundamental components of attention. *Ann. Rev. Neurosci.* 30, 57–78. doi: 10.1146/annurev.neuro.30.051606.094256

Larson, E., and Lee, A. K. C. (2013). The cortical dynamics underlying effective switching of auditory spatial attention. *NeuroImage* 64, 365–370. doi: 10.1016/j.neuroimage.2012.09.006

Laurienti, J., Burdette, J. H., Wallace, M. T., Yen, Y. F., Field, A. S., and Stein, B. E. (2002). Deactivation of sensory-specific cortex by cross-modal stimuli. *J. Cognit. Neurosci.* 14, 420–429. doi: 10.1162/089892902137361930

Ledoit, O., and Wolf, M. (2004). A well-conditioned estimator for large-dimensional covariance matrices. *J. Multiv. Anal.* 88, 365–411. doi: 10.1016/S0047-259X(03)00096-4

Lindquist, M. A., Loh, J. M., Atlas, L. Y., and Wager, T. D. (2009). Modeling the hemodynamic response function in fMRI: efficiency, bias and mis-modeling. *NeuroImage* 45, S187–198. doi: 10.1016/j.neuroimage.2008.10.065

Lolk, A. (2013). *Diagnostic and Statistical Manual of Mental Disorders: DSM-5™*, 5th Edn. Arlington, VA: American Psychiatric Publishing, Inc., 947.

Luke, R., Larson, E., Shader, M. J., Innes-Brown, H., Van Yper, L., Lee, A. K., et al. (2021). Analysis methods for measuring passive auditory fNIRS responses generated by a block-design paradigm. *Neurophotonics* 8:025008. doi: 10.1117/1.NPh.8.2.025008

Maddox, R. K., Atilgan, H., Bizley, J. K., and Lee, A. K. (2015). Auditory selective attention is enhanced by a task-irrelevant temporally coherent visual stimulus in human listeners. *ELife* 4:e04995. doi: 10.7554/eLife.04995

Maddox, R. K., Billimoria, C. P., Perrone, B. P., Shinn-Cunningham, B. G., and Sen, K. (2012). Competing sound sources reveal spatial effects in cortical processing. *PLoS Biol.* 10:e1001319. doi: 10.1371/journal.pbio.1001319

Marco, E. J., Hinkley, L. B., Hill, S. S., and Nagarajan, S. S. (2011). Sensory processing in autism: a review of neurophysiologic findings. *Pediatric Res.* 69, 48R–54R. doi: 10.1203/PDR.0b013e3182130c54

Marrone, N., Mason, C. R., and Kidd, G. (2008). Evaluating the benefit of hearing aids in solving the cocktail party problem. *Trends Amp.* 12, 300–315. doi: 10.1177/1084713808325880

Martuzzi, R., Murray, M. M., Michel, C. M., and Thiran, J. P. P., Clarke, S., and Meuli, R. A. (2006). Multisensory interactions within human primary cortices revealed by BOLD dynamics. *Cereb. Cortex* 17, 1672–1679. doi: 10.1093/cercor/bhl077

McDermott, J. H. (2009). The cocktail party problem. *Curr. Biol.* 19, R1024–R1027. doi: 10.1016/j.cub.2009.09.005

Michalka, S. W., Kong, L., Rosen, M. L., Shinn-Cunningham, B. G., and Somers, D. C. (2015). Short-term memory for space and time flexibly recruits complementary sensory-biased frontal lobe attention networks. *Neuron* 87, 882–892. doi: 10.1016/j.neuron.2015.07.028

Michalka, S. W., Rosen, M. L., Kong, L., Shinn-Cunningham, B. G., and Somers, D. C. (2016). Auditory spatial coding flexibly recruits anterior, but not posterior, visuotopic parietal cortex. *Cereb. Cortex* 26, 1302–1308. doi: 10.1093/cercor/bhv303

Mihali, A., Young, A. G., Adler, L. A., Halassa, M. M., and Ma, W. J. (2018). A low-level perceptual correlate of behavioral and clinical deficits in ADHD. *Comp. Psychiatry* 2, 141–163. doi: 10.1162/CPSY\_a\_00018

Naseer, N., and Hong, K. S. (2015). fNIRS-based brain-computer interfaces: a review. *Front. Hum. Neurosci.* 9:3. doi: 10.3389/fnhum.2015.00003

Petro, L. S., Paton, A. T., and Muckli, L. (2017). Contextual modulation of primary visual cortex by auditory signals. *Philos. Trans. Royal Soc. B Biol. Sci.* 372, 20160104. doi: 10.1098/rstb.2016.0104

Pollonini, L., Olds, C., Abaya, H., Bortfeld, H., Beauchamp, M. S., Oghalai, J. S., et al. (2014). Auditory cortex activation to natural speech and simulated cochlear implant speech measured with functional near-infrared spectroscopy. *Hearing Res.* 309, 84–93. doi: 10.1016/j.heares.2013.11.007

Scholkmann, F., and Wolf, M. (2013). General equation for the differential pathlength factor of the frontal human head depending on wavelength and age. *J. Biomed. Optics* 18:105004. doi: 10.1117/1.JBO.18.10.105004

Serenes, J. T., Shomstein, S., Leber, A. B., Golay, X., Egeth, H. E., Yantis, S., et al. (2005). Coordination of voluntary and stimulus-driven attentional control in human cortex. *Psychol. Sci. in Cognition* 16, 114–122. doi: 10.1111/j.0956-7976.2005.00791.x

Shomstein, S., and Yantis, S. (2006). Parietal cortex mediates voluntary control of spatial and nonspatial auditory attention. *J. Neurosci.* 26, 435–439. doi: 10.1523/JNEUROSCI.4408-05.2006

Smith, D. V., Davis, B., Niu, K., Healy, E. W., Bonilha, L., Fridriksson, J., et al. (2010). Spatial attention evokes similar activation patterns for visual and auditory stimuli. *J. Cognit. Neurosci.* 22, 347–361. doi: 10.1162/jocn.2009.21241

Steinmetzger, K., Shen, Z., Riedel, H., and Rupp, A. (2020). Auditory cortex activity measured using functional near-infrared spectroscopy (fNIRS) appears to be susceptible to masking by cortical blood stealing. *Hearing Res.* 396, 108069. doi: 10.1016/j.heares.2020.108069

Tian, X., Liu, Y., Guo, Z., Cai, J., Tang, J., Chen, F., et al. (2021). Cerebral representation of sound localization using functional near-infrared spectroscopy. *Front. Neurosci.* 15:739706. doi: 10.3389/fnins.2021.739706

Van der Zwaag, W., Gentile, G., Gruetter, R., Spierer, L., and Clarke, S. (2011). Where sound position influences sound object representations: a 7-T fMRI study. *NeuroImage* 54:32. doi: 10.1016/j.neuroimage.2010.10.032

von Lüthmann, A., Ortega-Martinez, A., Boas, D. A., and Yücel, M. A. (2020). Using the general linear model to improve performance in fNIRS single trial analysis and classification: a perspective. *Front. Hum. Neurosci.* 14:30. doi: 10.3389/fnhum.2020.00030

Wu, C. T., Weissman, D. H., Roberts, K. C., and Woldorff, M. G. (2007). The neural circuitry underlying the executive control of auditory spatial attention. *Brain Res.* 1134, 187–198. doi: 10.1016/j.brainres.2006.11.088

Yücel, M. A., Selb, J., Cooper, R. J., and Boas, D. A. (2014). Targeted principle component analysis: a new motion artifact correction approach for near-infrared spectroscopy. *J. Innov. Optical Health Sci.* 7:1350066. doi: 10.1142/S1793545813500661

Zhang, M., Alamatsaz, N., and Ihlefeld, A. (2021). Hemodynamic responses link individual differences in informational masking to the vicinity of superior temporal gyrus. *Front. Neurosci.* 15:675326. doi: 10.3389/fnins.2021.675326

Zhang, M., Mary Ying, Y. L., and Ihlefeld, A. (2018). Spatial release from informational masking: evidence from functional near infrared spectroscopy. *Trends Hearing* 22:2331216518817464. doi: 10.1177/2331216518817464